

Short-Term Environmental Conditioning Enhances Tumorigenic Potential of Triple-Negative Breast Cancer Cells

Samantha S. Eckley^{1#}, Johanna M. Buschhaus^{2,3}, Brock A. Humphries³, Tanner H. Robison^{2,3}, Kathryn E. Luker², and Gary D. Luker^{2,3,4}

¹Unit for Laboratory Animal Medicine, University of Michigan Medical School, Ann Arbor, MI; ²Department of Biomedical Engineering, University of Michigan College of Engineering and Medical School, Ann Arbor, MI; ³Department of Radiology Center for Molecular Imaging, University of Michigan Medical School, Ann Arbor, MI; and ⁴Department of Microbiology and Immunology, University of Michigan Medical School, Ann Arbor, MI

Corresponding Author:

Gary D. Luker, MD
University of Michigan College of Engineering and Medical School, 109
Zina Pitcher Place, A524 BSRB, Ann Arbor, MI 48109;
E-mail: gluker@umich.edu

Key Words:

Fluorescence, bioluminescence, signaling, breast cancer
Abbreviation: FBS, fetal bovine serum, EGF, epidermal growth factor, HMF, human
mammary fibroblasts, AUC, area under the curve

ABSTRACT

Tumor microenvironments expose cancer cells to heterogeneous, dynamic environments by shifting availability of nutrients, growth factors, and metabolites. Cells integrate various inputs to generate cellular memory that determines trajectories of subsequent phenotypes. Here we report that short-term exposure of triple-negative breast cancer cells to growth factors or targeted inhibitors regulates subsequent tumor initiation. Using breast cancer cells with different driver mutations, we conditioned cells lines with various stimuli for 4 hours before implanting these cells as tumor xenografts and quantifying tumor progression by means of bioluminescence imaging. In the orthotopic model, conditioning a low number of cancer cells with fetal bovine serum led to enhancement of tumor-initiating potential, tumor volume, and liver metastases. Epidermal growth factor and the mTORC1 inhibitor ridaforolimus produced similar but relatively reduced effects on tumorigenic potential. These data show that a short-term stimulus increases tumorigenic phenotypes based on cellular memory. Conditioning regimens failed to alter proliferation or adhesion of cancer cells in vitro or kinase signaling through Akt and ERK measured by multiphoton microscopy in vivo, suggesting that other mechanisms enhanced tumorigenesis. Given the dynamic nature of the tumor environment and time-varying concentrations of small-molecule drugs, this work highlights how variable conditions in tumor environments shape tumor formation, metastasis, and response to therapy.

INTRODUCTION

Heterogeneous perfusion creates distinct regional and temporal microenvironments within tumors (1, 2). Spatial disparities exist between the periphery and center of a tumor, with the periphery typically having better perfusion and greater temporal variability (2). Fluctuations in blood flow and intermittent perfusion of blood vessels in a tumor occur on time scales of minutes to hours (3, 4), generating perfusion mismatches that increase with tumor size (4). Chaotic, disorganized vasculature in tumors (5, 6) generates gradients of oxygen and nutrients (7–9), altering functions and metabolism of both cancer and stromal cells (10–13). For example, areas of poor perfusion result in hypoxic and acidic environments (1, 14) that promote aggressive disease and contribute toward resistance to radiotherapies and chemotherapies (15–18).

Changes in environmental conditions, including availability of nutrients, biochemical signals, and mechanics, generally are

considered to influence only immediate responses of cells. However, short-term inputs also alter intracellular states of cells, establishing memories of past conditions that regulate future outputs and functions (19–22). Both computational models of cell signaling (23) and experimental systems show cellular memory in bacterial (20) and mammalian cells (19, 21, 22). Stimuli on time scales of minutes to days (19, 21) can generate cellular memory through mechanisms including transcription and protein modifications, resulting in quantifiable, phenotypic changes in cellular behaviors. Thus, transient signals to a cell may influence the cellular state to produce long-term phenotypic consequences.

One mechanism producing cellular memory arises from shifting the ability of cells to signal in response to a biochemical stimulus. Our group recently established a single-cell

Current affiliation: University of Iowa, Office of Animal Resources, Iowa City, IA.

model of signaling through chemokine receptor CXCR4 to the PI3K/Akt/mTOR (PI3K) and Raf/MEK/ERK (MEK) pathways (24). Dysregulated signaling through these pathways drives breast cancer and multiple other malignancies. For instance, mutations activating the PI3K pathway occur in ~70% of breast cancers (25). Breast cancers also commonly exhibit constitutive activation of MEK signaling even though mutation in this pathway occur in only 2–10% of breast cancers (26–29). Our computational model predicted heterogeneity and single-cell dynamics within a population of breast cancer cells given known environmental conditions and signaling inputs. This work also revealed that previous environmental conditions generated short-term cellular memory, shifting states of responsiveness to signaling. In particular, growth factor conditioning and treatment with inhibitors of MEK and mTOR potentiated subsequent CXCR4 signaling in cell culture.

Although our prior work showed generation of memory to environmental conditioning in cell culture, we could not establish functional significance of cellular memory. Here, we investigated the effects of environmental conditioning on tumor- and metastasis-initiating potentials of breast cancer cells in a mouse model of human breast cancer. This approach leverages endogenous murine CXCL12, which we and others have shown promotes growth of orthotopic tumors and metastasis of both mouse and human breast cancer cells (30, 31). We hypothesized that inputs potentiating signaling in vitro in our prior study would increase tumorigenic potential of breast cancer cells. Here we show enhanced tumorigenic behavior, resulting in higher tumor formation, growth, and metastasis. These results further establish that cells retain the memory of short-term changes in environmental conditions that cause long-term biological effects in cancer.

METHODS

Cell Culture

We cultured the triple-negative human breast cancer cell line MDA-MB-231 (ATCC, Manassas, VA) as described previously (44). We stably expressed CXCR4-BFP and click beetle green luciferase in these cells using recombinant lentiviral vectors and kinase translocation reporters (KTRs) for Akt and ERK with a transposon vector system (PiggyBac Transposon, System Biosciences, Palo Alto, CA) (24). The transposon vector also expresses histone 2B fused to mCherry (H2B-mCherry) to define the nucleus of each cell. We cultured human mammary fibroblasts (provided by Daniel Hayes, University of Michigan, Ann Arbor, MI) as described for MDA-MB-231 cells. Vari-068 cells (provided by Sofia Merajver, University of Michigan, Ann Arbor, MI) are patient-derived, triple-negative breast cancer cells adapted to cell culture (37). We used a recombinant lentivirus to stably express click beetle green luciferase in Vari-068 cells and cultured them as described previously (38). We used all cells within 3 months after resuscitation from frozen stocks.

Cell Conditioning

We seeded cells (1.2×10^5 MDA-MB-231, or 2.0×10^5 Vari-068) in 35-mm dishes with a 20-mm glass bottom (Cellvis, Mountain View, CA) in 1.5 mL of imaging base media (FluoroBrite Dulbecco's Modified Eagle Medium media (A1896701, ThermoFisher Scientific, Waltham, MA), 1% GlutaMax, 1% PenStrep and 1% sodium pyruvate) supplemented with 10% fetal bovine serum

(HyClone). Two days after seeding, we changed dishes to 2.0 imaging base media with 1% FBS for all cell types. The next day, we conditioned breast cancer cells by adding FBS (final concentration, 10%), EGF (final concentration, 30 ng/mL or 300 ng/mL as listed in various figure legends) (R&D Systems, Minneapolis, MN), ridaforolimus (Selleck Chemicals, Houston, TX; final concentration, 10 nM), or trametinib (Selleck Chemicals; final concentration, 100 nM) to their existing media and incubated for 4 hours. Control cells remained in the same medium without the addition of a conditioning stimulus.

Cellular Growth and Adhesion Assays

To quantify proliferation, we conditioned cells as described above and then detached the cells with 0.25% trypsin. We seeded 10^3 MDA-MB-231 cells in imaging base media supplemented with 1% FBS into a 96-well plate in quadruplicate. After incubating cells for approximately 2 hours, we imaged luciferase activity (day 0) in selected wells using an IVIS Lumina LT Series III (Perkin Elmer, Waltham, MA) with medium binning and exposure of 1–5 minutes as described previously (45). We performed imaging studies daily for an additional 2 days and quantified imaging data as photon flux with Living Image 4.5.5.

We quantified the effects of conditioning stimuli on adhesion of MDA-MB-231 cells to human mammary fibroblasts (HMFs) as described previously (44). In brief, we seeded 10^5 HMFs per well in a 24-well plate and cultured cells for 2 days to produce a confluent monolayer. We conditioned MDA-MB-231 cells as described and then removed cells with 0.25% trypsin. We washed HMFs with PBS and added 2.5×10^5 MDA-MB-231 cells per well in imaging base media supplemented with 1% FBS. After incubating cells 15 minutes at 37°C, we removed nonadherent MDA-MB-231 cells with PBS and visualized adherent cells by fluorescence imaging.

Animals

The University of Michigan Institutional Animal Care and Use Committee approved all procedures involving animals. We performed all experimental procedures in accordance with institutional guidelines and regulations. We used 17- to 25-week-old female NSG mice (The Jackson Laboratory, Bar Harbor, ME) housed in autoclaved positive pressure, positive/negative control individually ventilated cages (P/NV IVC; Allentown, Allentown, NJ) with corn cob bedding (The Andersons, Maumee, OH) and provided with reverse osmosis-deionized water through automated water systems (Edstrom, Waterford, WI). Animal-housing rooms maintained a cycle of 12 hours of light/12 hours of dark, with relative humidity at 30–70% and temperature of $72 \pm 2^\circ\text{F}$ ($22.2 \pm 1.1^\circ\text{C}$). The health surveillance program for specific pathogen free colonies included quarterly testing of dedicated soiled-bedding sentinel animals via fecal and perianal swab polymerase chain reaction or serology and polymerase chain reaction of exhaust plenum swabs for fur mites. Health surveillance results indicated that the mice were negative for mouse rotavirus, mouse hepatitis virus, minute virus of mice, ectromelia virus, Theiler mouse encephalomyelitis virus, lymphocytic choriomeningitis virus, mouse adenovirus, mouse parvovirus, mouse polyomavirus, pneumonia virus of mice, reovirus, Sendai virus, *Mycoplasma pulmonis*, pinworms (*Syphacia spp.* and *Aspicularis spp.*), and fur mites (*Myobia musculi*, *Myocoptes musculinus*, and *Radfordia affinis*).

Table 1. Tumor Formation after Bilateral Injection of MDA-MB-231 Cells at Different Cell Dosages after Conditioning^a

Condition	Number of Cells Injected		
	10 ²	10 ³	10 ⁴
Control	0/8 (0%)	16/24 (67%)	17/18 (94%)
FBS	4/8 (50%)	24/24 (100%)**	18/18 (100%)

^aDisplayed as number of tumors formed/number of injections (percent tumors formed); ***P* = .0039 versus control by Fisher exact test.

Orthotopic Mouse Model of Breast Cancer

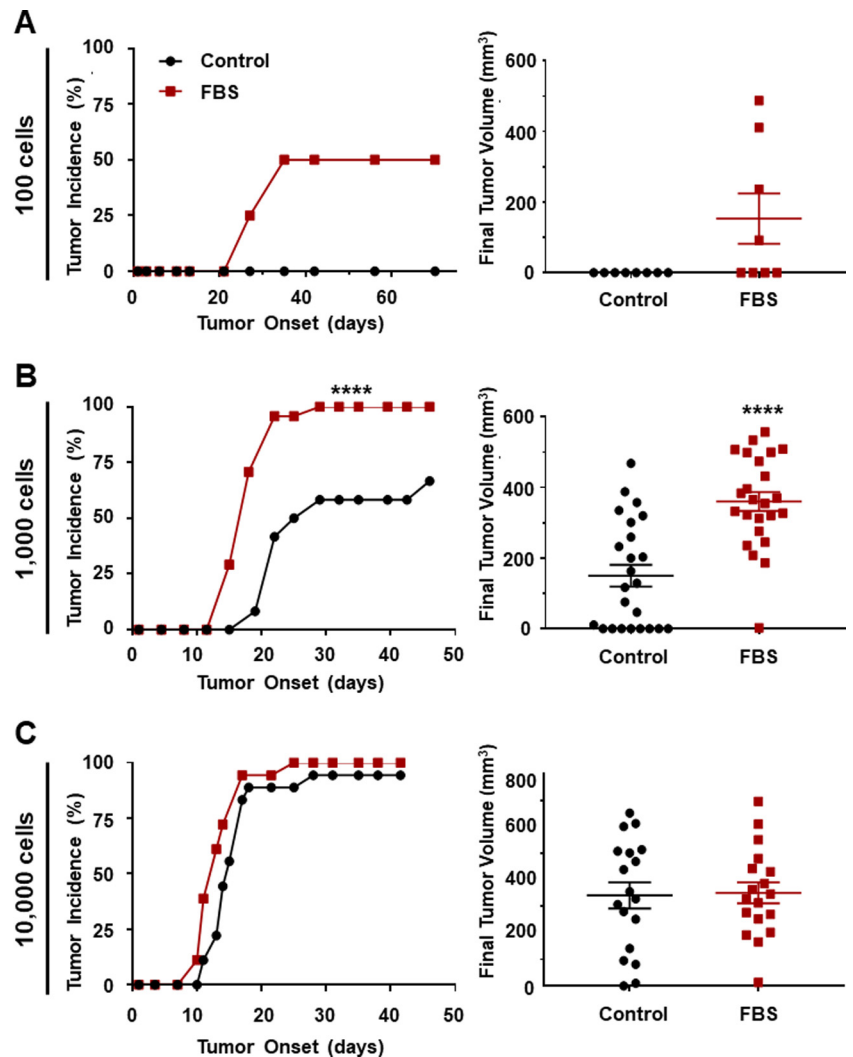
We conditioned MDA-MB-231 or Vari-068 cells as described above, harvested the cells with a cell dissociation buffer, and then injected 10², 10³, or 10⁴ MDA-MB-231 or 10³ or 10⁴ Vari-068 cells bilaterally into the fourth inguinal mammary fat of female NSG mice (day 0) (46). We quantified tumor growth by caliper measurements in 3 dimensions and bioluminescence imaging (IVIS Spectrum, Perkin-Elmer) at regular intervals as

described previously (31). We defined experimental endpoints as time when FBS-conditioned tumors reached ~1.0 cm in diameter or 70–80 days after implantation, whichever occurred first. At the endpoint, we measured tumor volume and visually inspected the organs for metastases. In select experiments, we removed organs and assessed the metastases by means of bioluminescence. We considered an organ positive for metastases if bioluminescence exceeded the background signal by at least 2-fold.

In Vivo Fluorescence Imaging of Cancer Cells in the Orthotopic Mouse Tumor Model

We injected 10⁶ control or FBS-conditioned MDA-MB-231 cells into the left fourth mammary pad of female NSG mice anesthetized with isoflurane and began intravital microscopy ~5–30 minutes after injection. We imaged injected breast cancer cells in the mammary fat pads with an Olympus FVMPE-RS upright microscope, 25× NIR-corrected objective, and 3-channel detection (cyan [480/40], yellow [540/40], red [641/75]). We used 940 nm excitation for Aquamarine and mCitrine and 1040-nm excitation for mCherry with laser power set at 15%. We analyzed images using in-house

Figure 1. Fetal bovine serum (FBS) conditioning enhances tumor-initiating potential at low cell numbers. We conditioned MDA-MB-231 cells with FBS or control for 4 hours before implanting 10² (n = 2 mice for tumor incidence and 4 mice for final tumor volume) (A), 10³ (n = 12 mice) (B), or 10⁴ (n = 9 mice) (C) bilaterally into the fourth mammary fat pads of NSG (NOD scid gamma) mice on day 0. For each number of injected cells, graphs show the percentage of implantations that formed tumors over time (left) and the scatterplots with mean ± SEM for final tumor volume measured in 3 dimensions with calipers (right). We terminated experiments at 45–52 days for injections of 10² cells, 45–47 days for 10³ cells, and 32–50 days for 10⁴ cells. *****P* < .0001 by 2-tailed *t* test with the Welch correction for FBS versus control tumor onset and volume.



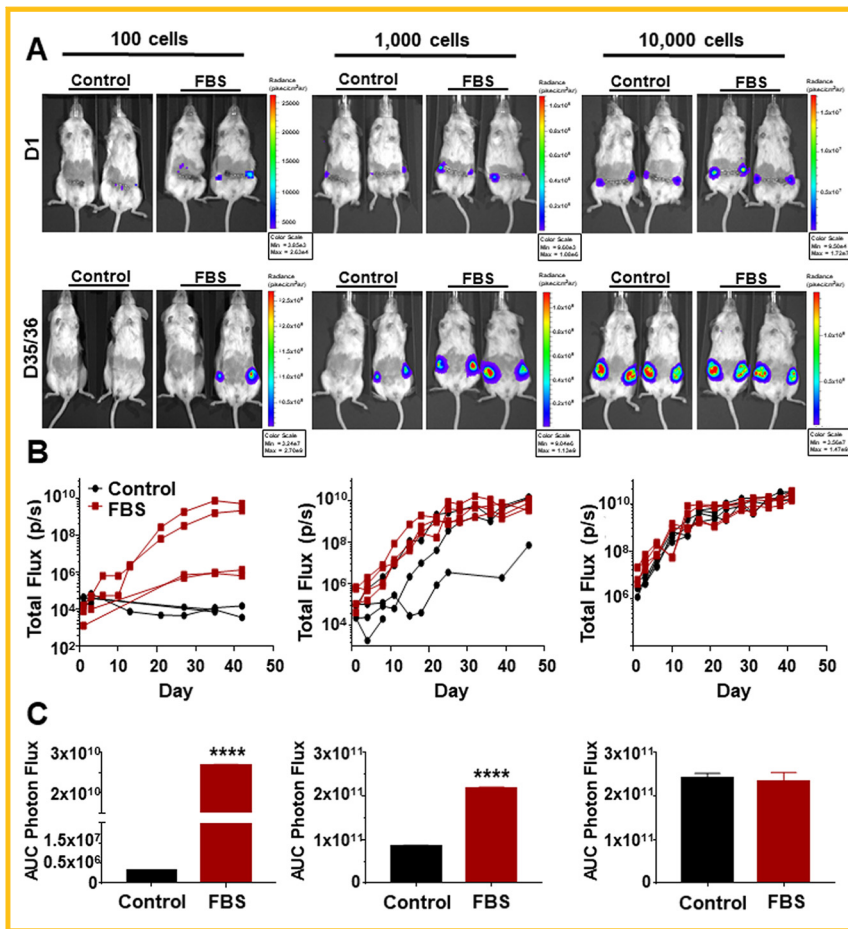


Figure 2. FBS conditioning increases tumor growth beginning 1 day after implantation. Following conditioning with FBS or control as described in Figure 1, we implanted 10^2 , 10^3 , or 10^4 MDA-MB-231 cells bilaterally into fourth mammary fat pads of NSG mice on day 0 (A). Panel displays representative bioluminescence images of primary mammary tumors from mice in each group on day 1 and days 35–36 after implantation. Images show photon flux from bioluminescence on a pseudocolor scale, with red and blue representing the highest and lowest values, respectively. Quantified bioluminescence signal over time for representative individual tumors depicted in (A) corrected for background signal (B). Graphs show mean area-under-the-curve for photon flux + SEM through 47 d for injections of 10^2 ($n = 4$ mice), 10^3 ($n = 12$ mice), and 10^4 ($n = 9$ mice) MDA-MB-231 cells (C). **** $P < .0001$ by 2-tailed t test with Welch's correction for FBS versus control.

MATLAB code to calculate the ratio of median fluorescence intensities in cytoplasm to the nucleus, expressed as the log₂ of the cytoplasm to the nucleus, for Akt and ERK KTRs (24). We output data as pairs of Akt and ERK KTR measurements for each of the ~200 to 400 cells in an image.

Metastatic Mouse Model of Breast Cancer

To simulate systemic metastases, we conditioned MDA-MB-231 as described above, harvested the cells with a cell dissociation buffer, and then injected 10^4 MDA-MB-231 cells into the left ventricle of the heart of the female NSG mice (day 0) under isoflurane anesthesia (47). We used bioluminescence imaging (IVIS Spectrum, Perkin-Elmer) to measure the metastatic burden and quantified the extent of disease based on bioluminescence of the thorax and abdomen over time. We euthanized the mice at the endpoint (day 33) or earlier (days 27–30) based on clinical presentation. We visually inspected the organs for metastases, and then we removed the organs to detect metastases by bioluminescence imaging. We also harvested bone marrow from the lower extremities as described (48) and evaluated the bioluminescence after culture in Dulbecco's Modified Eagle Medium for 7 days.

Statistical Analysis

We analyzed data using GraphPad Prism (San Diego, CA). Before statistical analyses, we tested data for normality using the

D'Agostino & Pearson normality test or the Shapiro–Wilk normality test, if the n was too small for the former. We analyzed tumor volumes, tumor onset, AUC, and organ metastases for control versus FBS-conditioned cells with unpaired 2-tailed t test for parametric data with Welch's correction for unequal variance, or Mann–Whitney test if nonparametric. We used Fisher exact test to assess tumor formation incidence. We analyzed tumor volumes and tumor onset with EGF and inhibitor conditioning, growth assay, and adhesion assay using 1-way ANOVA followed by Tukey multiple comparisons test for parametric data or Kruskal–Wallis test followed by the Dunn multiple comparisons test for nonparametric data. We considered a P -value of $< .05$ as statistically significant.

RESULTS

Fetal Bovine Serum Conditioning Enhances Tumor-Initiating Potential at Low Numbers of Cells

Our previous cell culture work showed differences in signaling responsiveness after conditioning with fetal bovine serum (FBS) (24). To determine the effects on tumor formation and growth, we first assessed the effects of conditioning on the tumor-initiating ability of MDA-MB-231 human breast cancer cells. We conditioned cells with no additives (control) or 10% FBS for 4 hours before injecting 10^2 , 10^3 , or 10^4 cells bilaterally into the fourth mammary fat pads of female NSG (NOD scid gamma) mice (10^2 cells: $n = 4$ mice; 10^3 cells: $n = 12$ mice; and 10^4 cells: $n = 9$ mice per condition).

As expected, higher cell dosages generated greater frequencies of tumor formation for both control and FBS-conditioned cells (Table 1). FBS-conditioned cells showed earlier onset of tumor formation (Figure 1, A–C; 10^3 cells, $P < .0001$) and a higher percentage of tumors formed (Table 1; 10^2 cells, $P = .0769$; 10^3 cells, $P = .0039$) for all cell dosages with greater effects evident at 10^2 and 10^3 cells. For injections with 10^2 MDA-MB-231 cells, tumors were formed only from cells conditioned with FBS. Conditioning with FBS before implantation of 10^3 but not 10^4 cells also increased final volumes of tumors relative to control ($P < .0001$).

FBS Conditioning Increases Early Tumor Growth

Using bioluminescence imaging to assess tumor growth, we observed differences between control and FBS-conditioned cells within 24 hours of implantation for groups with implanted 10^2 and 10^3 cells (Figure 2A). These disparities persisted over time (Figure 2B). We quantified the overall bioluminescence signals for the full experiment using area-under-the-curve (AUC) analysis. Both 10^2 and 10^3 cell implantations showed significantly higher AUC ($P < .0001$) for FBS-conditioned cells relative to control, indicating higher cumulative growth.

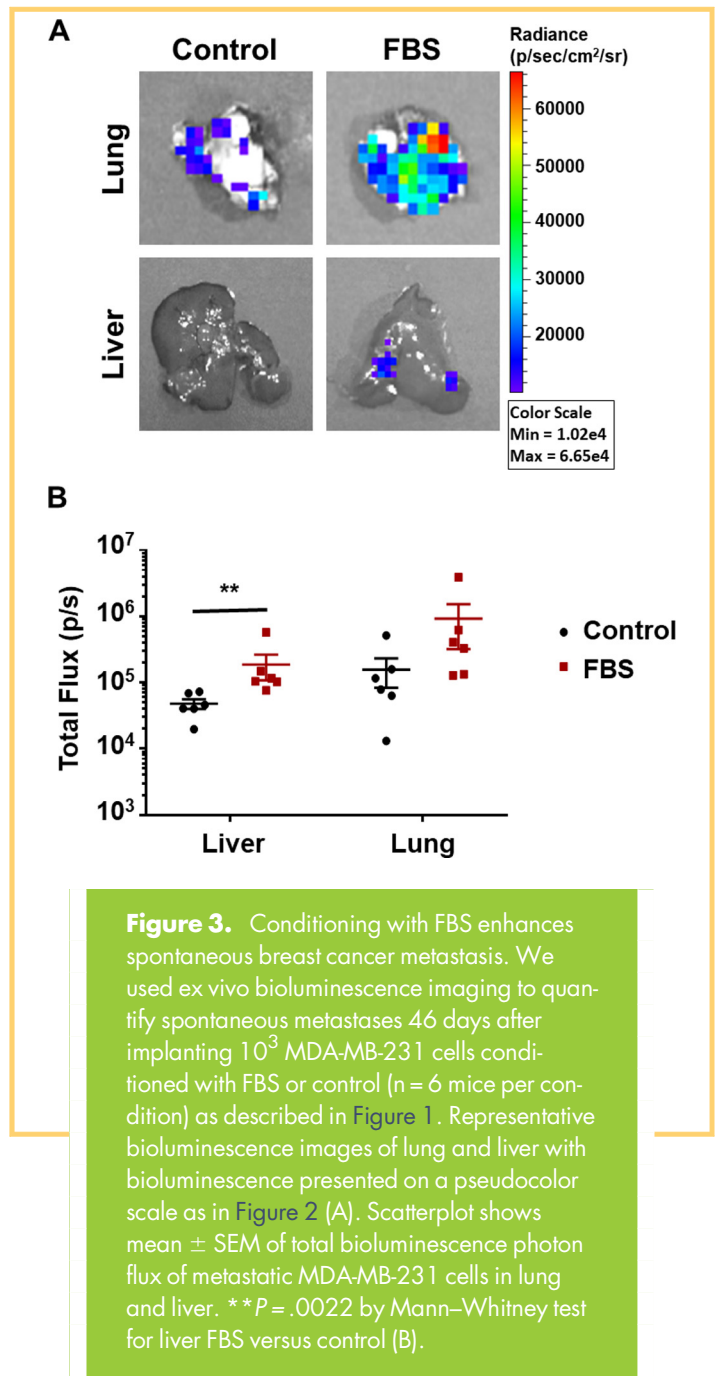
Metastatic Potential of Cells Varies with Conditioning and Experimental Model

We also analyzed spontaneous metastases to lung and liver, 2 common sites of metastatic breast cancer, in mice injected orthotopically with 10^3 MDA-MB-231 cells ($n = 6$ mice per condition). Ex vivo bioluminescence imaging showed higher signal in liver ($P = .0022$) and lung ($P = .0649$) in mice implanted with FBS-conditioned cells compared with control (Figure 3, A and B; Table 2). One mouse with FBS-conditioned cells also showed splenic metastasis (Table 2).

To focus on steps in metastasis independent of an orthotopic tumor, we injected 10^4 cells into the left ventricle of the heart to disseminate breast cancer cells systemically ($n = 5$ mice per condition). Control and FBS-conditioned cells initially showed bioluminescent signal in the thorax on day 1 (Figure 4). However, after 15 days, cellular bioluminescence signal distributed heterogeneously with substantial signal in select mice. Two mice with control-conditioned cells had abundant signals in the abdomen, distal limbs, and cervical region, while 1 mouse with FBS-conditioned cells displayed strong signal in the thorax (Figure 4). By the endpoint, control and FBS-conditioned cells showed a similar incidence of organ metastases (Table 2). The mouse with FBS-conditioned cells and abundant thoracic signal was not assessed for organ luminescence owing to premature euthanasia, but this animal exhibited visible lung metastases. These results indicate greater effects of conditioning stimuli on tumor progression from an orthotopic mammary environment.

Conditioning With Epidermal Growth Factor Enhances Tumor-Initiating Potential over Control

Because FBS contains a variety of different growth factors, we focused on epidermal growth factor (EGF) as a single, defined cytokine known to promote proliferation and tumor growth. We conditioned cells with 30 ng/mL EGF, a concentration that enhanced signaling responsiveness to an extent similar to FBS in our previous *in vitro* experiments (24). EGF-conditioned cells formed tumors earlier after implantation ($P = .0480$) but with



comparable overall incidence to control MDA-MB-231 cells ($n = 6$ mice per condition). Conditioning with EGF produced lesser effects on tumor-initiation than FBS, indicating that multiple cytokines contribute to observed effects of conditioning with FBS (Figure 5A; Table 3). Both EGF and control cells showed comparable bioluminescence over time, with this value being lower in both groups than that in the cells conditioned with FBS (Figure 5B). We observed no significant difference in final tumor volumes between EGF and control cells (Figure 5C). FBS-conditioned cells again showed significantly higher tumor volumes than control cells ($P = .0040$) and trended higher than EGF-conditioned MDA-MB-231 cells ($P = .0589$).

Table 2. Frequency of Mice with Metastases of MDA-MB-231 Cells after Conditioning and Implantation in the Orthotopic or Metastatic Mouse Model^a

Model	Condition	Organ			
		Lung	Liver	Spleen	Bone Marrow
Orthotopic	Control	5/6 (83%)	2/6 (67%)	0/6 (0%)	NA ^b
	FBS	6/6 (100%)	6/6 (100%)	1/6 (17%)	NA
Metastatic	Control	5/5 (100%)	4/5 (80%)	2/5 (40%)	1/4 (25%) ^c
	FBS	5/5 (100%)	3/4 (75%) ^b	2/4 (50%) ^b	0/4 (0%) ^d

^a Displayed as number of metastases formed/number of mice (percent tumors formed).

^b NA: Not applicable.

^c Unable to collect bone marrow from one mouse.

^d Unable to image organs due to early euthanasia in one mouse. Visible lung metastases present.

Conditioning With Targeted Inhibitors Variably Affects Tumor Formation and Growth

Our previous study combining computational modeling and cell culture experiments utilized ridaforolimus and trametinib, inhibitors of mTORC1 and MEK, respectively, to shift responsiveness of cells to signaling. Ridaforolimus activates both MEK and PI3K pathways (32, 33), while inhibition of MEK with trametinib produces compensatory activation of PI3K signaling (24, 34). To test the effects on tumor initiation and growth, we conditioned MDA-MB-231 cells with ridaforolimus or trametinib before implanting 10^3 cells into mammary fat pads of mice ($n = 6$ mice per condition). Conditioning with ridaforolimus increased the incidence of tumor initiation relative to control, albeit to a lesser extent than conditioning with FBS (Figure 6A; Table 4). By comparison, trametinib modestly delayed the time to tumor formation while ultimately reaching the same incidence as control. These data suggest that conditioning stimuli activating both PI3K and MEK signaling pathways prime the cells for tumor formation to a greater extent than that activating PI3K alone. For tumors that formed, bioluminescence imaging data over the course of tumor growth showed similar kinetics, with the highest signal obtained from cells conditioned with FBS (Figure 6B). Final tumor volumes ranged substantially

with significantly higher mean volumes for FBS than for control ($P = .0399$) (Figure 6C). Cells conditioned with FBS also had higher final mean volumes than those conditioned with trametinib ($P = .0310$) (Figure 6C).

Conditioning Treatments do not Alter Population-Level Proliferation or Adhesion of Cancer Cells in Cell-Based Assays

To investigate mechanisms through which conditioning regimens alter tumor-initiating potential of breast cancer cells, we performed in vitro assays for proliferation and adhesion of MDA-MB-231 cells. We measured effects of various conditioning stimuli on proliferation using bioluminescence to quantify increases in the numbers of cells over 2 days. Conditioning with trametinib produced significantly lower proliferation after 2 days (Figure 7A; $P = .0261$), consistent with the observed delay in tumor initiation. However, conditioning with FBS, EGF, or ridaforolimus did not change proliferation relative to control. We also measured the effects of conditioning on adhesion of MDA-MB-231 cells to human mammary fibroblasts. We observed no differences in adhesion among all conditions, even in experiments in which we increased the concentration of ridaforolimus by 10-fold (Figure 7B).

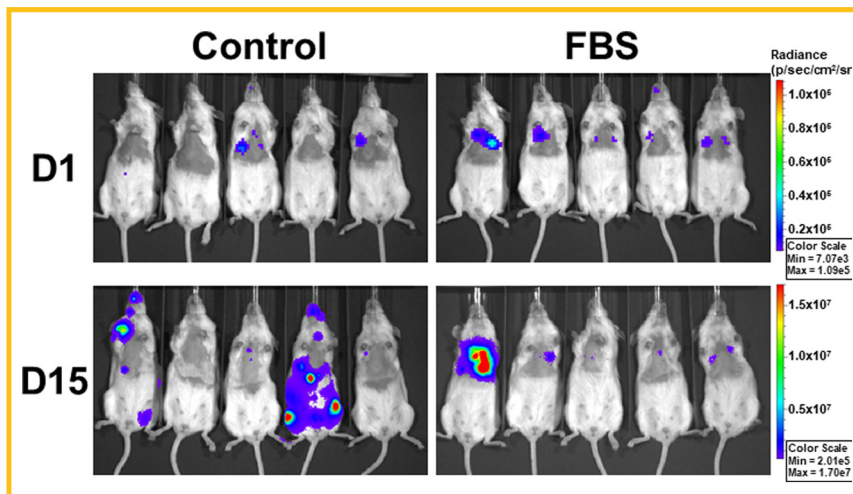


Figure 4. Experimental metastases display variability in organ site and intensity over time. We conditioned MDA-MB-231 cells with FBS or control for 4 hours before intracardiac injection of 10^4 cells per mouse ($n = 5$ mice per condition) to experimentally produce metastases. Presented images show pseudocolor displays of bioluminescence from each group of mice on days 1 and 15 after injection. We used different ranges of pseudocolor scales for days 1 and 15 to account for the large increase in signal over time.

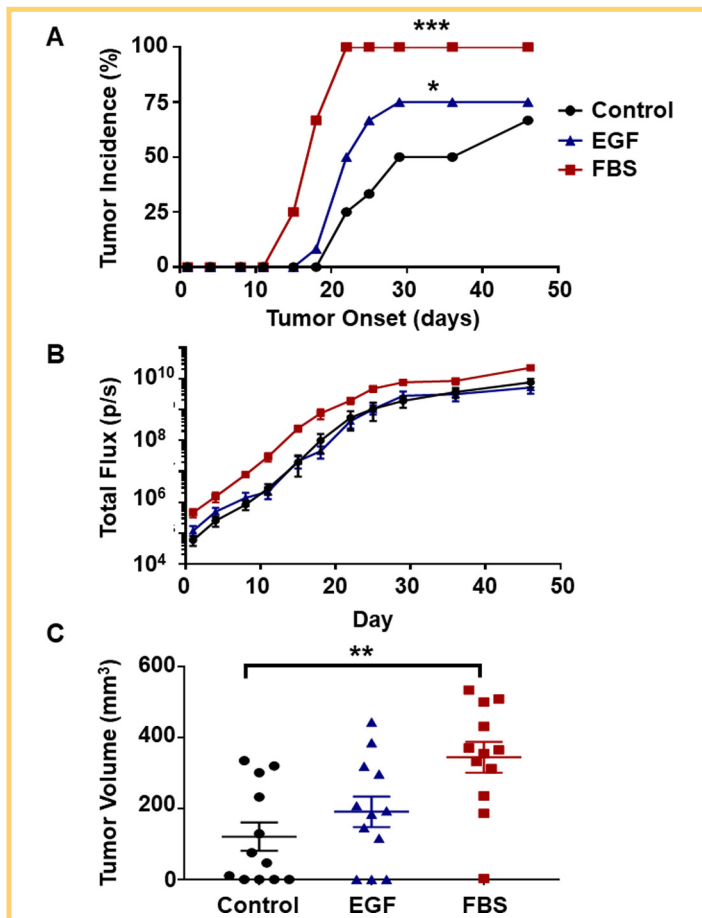


Figure 5. Epidermal growth factor (EGF) conditioning enhances onset of breast tumor formation. We conditioned MDA-MB-231 cells with EGF (30 ng/ml), FBS, or control for 4 hours before orthotopic implantation of 10^3 cells per mammary fat pad ($n = 6$ mice per condition). Graph displays tumor incidence over time for each group (A). $*P = .048$ for EGF versus control and $***P = .0006$ for FBS versus control tumor onset by 1-way ANOVA. Mean \pm SEM for photon flux over time in each group (B). Note log scale for total flux values. Scatterplot shows mean \pm SEM for final tumor volume on day 46 measured in 3 dimensions with calipers (C). $**P = .004$ for FBS versus control tumor volume by Kruskal–Wallis test.

Conditioning does not Alter Activities of Akt or ERK in Breast Cancer Cells Immediately after Injection into Mammary Fat Pads

We used fluorescent kinase translocation reporters to quantify activities of ERK and Akt in single MDA-MB-231 breast cancer cells (24, 35, 36). These reporters reversibly translocate from nucleus to cytoplasm upon phosphorylation, providing a quantitative readout of kinase activities for ERK and Akt. To assess the effects of FBS conditioning versus control on signaling by ERK

Table 3. Tumor Formation after Bilateral Injection of MDA-MB-231 Cells after Conditioning with EGF Compared to Control or FBS Conditioned Cells^a

Condition	Number of Cells Injected
	10^3
Control	8/12 (67%)
FBS	12/12 (100%)
EGF	9/12 (75%)

^a Displayed as number of tumors formed/number of injections (percent tumors formed).

and Akt in vivo, we implanted 10^6 cells into the left fourth mammary fat pad. Within 15 min of injection, we imaged kinase translocation reporters for ERK and Akt in living mice using 2-photon microscopy (Figure 8A). Imaging data revealed substantial overlap in activities of ERK and Akt between samples conditioned with FBS or control, indicating no significant population-level differences in signaling (Figure 8B).

FBS Conditioning Promotes Tumor Formation in Patient-Derived Vari-068 Breast Cancer Cells

To extend these studies to breast cancer cells with a different driver mutations, we used patient-derived, triple-negative Vari-068 cells (37, 38). Mutant PTEN in these cells activates PI3K, unlike MDA-MB-231 cells, with constitutive signaling through the MEK pathway. We conditioned Vari-068 cells with FBS, EGF, or control before implanting 10^3 or 10^4 cells into mammary fat pads of NSG mice ($n = 3$ mice per condition). For these studies, we used a higher concentration of EGF for conditioning because this growth factor activates signaling to a lesser extent in Vari-068 relative to MDA-MB-231 cells. Similar to studies with MDA-MB-231 cells, we observed greater differences in tumor formation with injections of 10^3 cells. Conditioning with FBS increased frequency ($P = .0152$) and reduced time to onset of tumor formation (Figure 9A; Table 5). For injections of 10^3 cells, conditioning with EGF also increased tumor formation relative to control, the latter of which produced no detectable tumors. Bioluminescence imaging over the course of the experiment also showed the same rank order of tumor growth for injections of 10^3 cells, while all groups injected with 10^4 cells exhibited similar tumor formation and growth (Figure 9B). Conditioning with FBS also significantly increased final tumor volume from injections of 10^3 cells relative to other groups ($P = .0167$) (Figure 9C). We observed a trend that failed to reach statistical significance for conditioning with FBS or EGF to produce larger tumors in mice injected with 10^4 cells. Overall, these results generally reproduce effects in MDA-MB-231 cells, suggesting a general effect of selected conditioning stimuli on tumor formation and growth.

DISCUSSION

Tumor cells reside in an ever-changing environment that influences their cellular state and subsequent phenotypic behaviors. Our work demonstrates that exposure to a single short-term

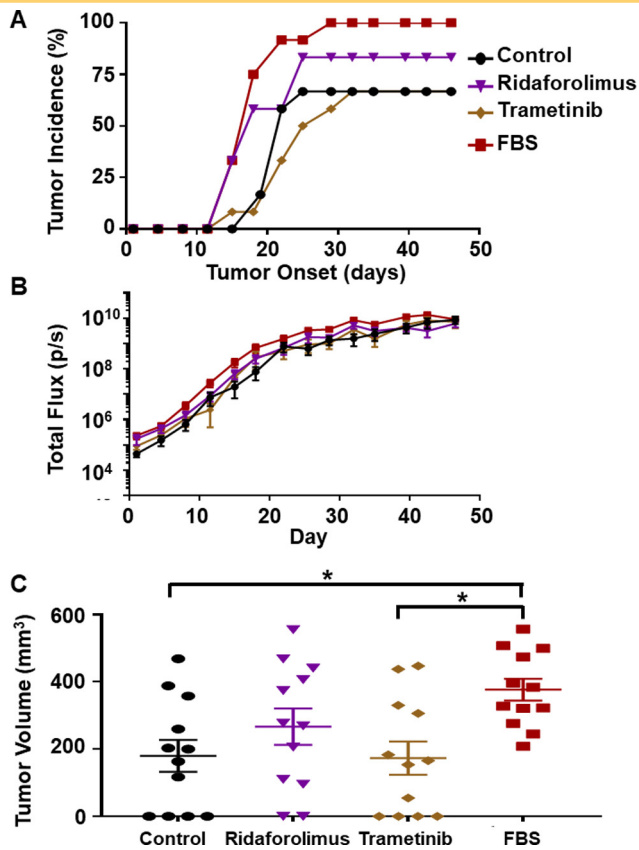


Figure 6. Conditioning with targeted inhibitors variably affects tumor formation and growth. We conditioned MDA-MB-231 cells with ridaforolimus (100 nM), trametinib (100 nM), FBS, or control for 4 hours before orthotopic implantation of 10^3 cells per mammary fat pad ($n = 6$ mice per condition). Graph shows percent incidence of tumors over time for each condition (A). Mean values \pm SEM for bioluminescence in each group over time (B). Note log scale for total flux. Scatterplot with mean \pm SEM for final tumor volume on day 46-47 measured in 3 dimensions with calipers (C). * $P = .040$ for FBS versus control and $P = .031$ for trametinib versus FBS by 1-way ANOVA.

stimulus regulated subsequent tumor initiation and progression in breast cancer. Conditioning with FBS produced striking differences in frequencies of tumor formation from limited numbers of cells with earlier onset of tumors, higher incidence, larger tumors, and more metastases in 2 cell lines with different driver mutations. Conditioning with the specific growth factor EGF and the inhibitor ridaforolimus also produced higher incidence and earlier onset of tumor formation from limited numbers of cells. Because FBS produced greater effects on these outcomes than EGF or ridaforolimus, our data suggest that conditioning stimuli promote tumor initiation and growth through multiple mechanisms.

Table 4. Tumor Formation after Bilateral Injection of MDA-MB-231 Cells after Conditioning with an mTORC1 (Ridaforolimus) or MEK (Trametinib) Inhibitor Compared to Control or FBS Conditioned Cells^a

Condition	Number of Cells Injected
	10^3
Control	8/12 (67%)
FBS	12/12 (100%)
Ridaforolimus	10/12 (83%)
Trametinib	8/12 (67%)

^a Displayed as number of tumors formed/number of injections (percent tumors formed).

These results link the phenomenon of cellular memory to past environmental inputs, which occurs in a variety of cells, from bacteria (20) to human cancers (19, 21,22). Multiple studies establish that culturing cancer cells in hypoxic conditions for several days improves subsequent tumor-initiating potential, invasion, and metastasis (19, 22). Another stimulus, TGF β , induces epithelial-to-mesenchymal transition in mouse mammary epithelial cells after a 5-minute pulse (21). For our studies, conditioning cells for 4 hours with a single stimulus of FBS, EGF, or mTORC1 inhibitor ridaforolimus promoted the initiation of orthotopic tumor implants in mammary fat pads of NSG mice. FBS contains a variety of nutrients and growth factors that likely regulate multiple intracellular pathways, while EGF may control a more limited subset of potential effectors of tumor formation and growth. Common effects of both FBS and EGF highlight the functions of growth factors in producing memory that ultimately decides the fate of a cell. Inhibition of mTORC1 with ridaforolimus activates 2 pathways important in breast cancer, MEK and PI3K (32, 33,38), providing mechanisms by which conditioning with this drug increases numbers of tumor-initiating cells and tumor initiation (39, 40). Because ongoing clinical trials in breast cancer include ridaforolimus, our data showing that this drug enhances tumor-initiating potential of breast cancer cells raise possible concerns for unexpected consequences of therapy. Combination therapies blocking both MEK and PI3K pathways potentially could overcome adverse effects of ridaforolimus, but such combinations currently produce unmanageable toxicities in patients (41-43). We did not test how long effects of conditioning persist in enhancing tumor initiation, but our cell-based studies indicate that memory of prior stimuli wanes by 7 hours (24). Our data also support short-term persistence of cellular memory to promote breast cancer. We observed the greatest differences on conditioning inputs on tumor incidence with lesser effects on subsequent growth of tumors.

We observed an unanticipated discrepancy between spontaneous metastases from orthotopic tumors versus an intracardiac injection model of experimental metastasis. Conditioning with FBS increased overall metastases from orthotopic tumors but not from intracardiac injections. This difference likely arises from the longer tumor growth interval and larger orthotopic tumor size in

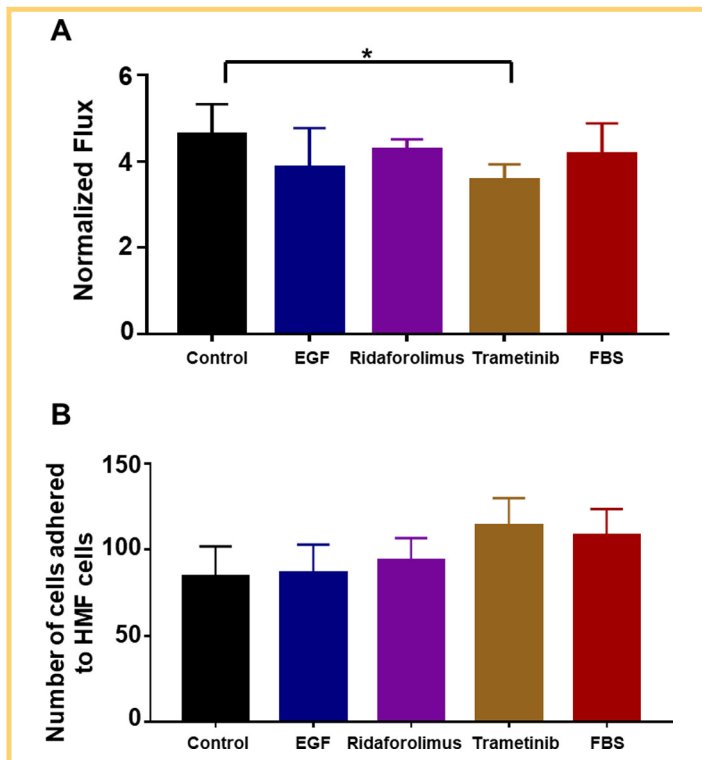


Figure 7. Conditioning treatments do not alter population-level proliferation or adhesion of cancer cells in cell-based assays. We conditioned MDA-MB-231 cells with EGF (30 ng/mL), ridaforolimus (100 nM), trametinib (100 nM), FBS, or control prior to seeding 10^3 cells per well in a 96-well plate ($n \geq 4$ per condition) (A). We normalized bioluminescence on days one and two to corresponding values on day 0 for each group. Graph shows mean + SEM for normalized bioluminescence on day 2 for each condition as a marker of proliferation. $*P = .0261$ for control versus trametinib by 1-way ANOVA. We conditioned cells with the same treatments listed in (A) and then seeded 2.5×10^5 cells per well onto confluent monolayers of human mammary fibroblasts (HMFs) in a 24-well plate (B). We washed off nonadherent cells with PBS after 15 minutes and then quantified the number of adherent breast cancer cells. Graph shows mean + SEM for cells adhering to breast cancer cells for each condition (EGF, 30 ng/mL; ridaforolimus, 100 nM; trametinib, 100 nM; FBS; or control) ($n \geq 10$ per condition).

mice with FBS-conditioned cells. There also may be site-specific conditioning effects on initial growth in the intracardiac model given the difference in the strong bioluminescent signal between metastatic sites. In the orthotopic model, the effects of conditioning likely ended before dissemination, accounting for no

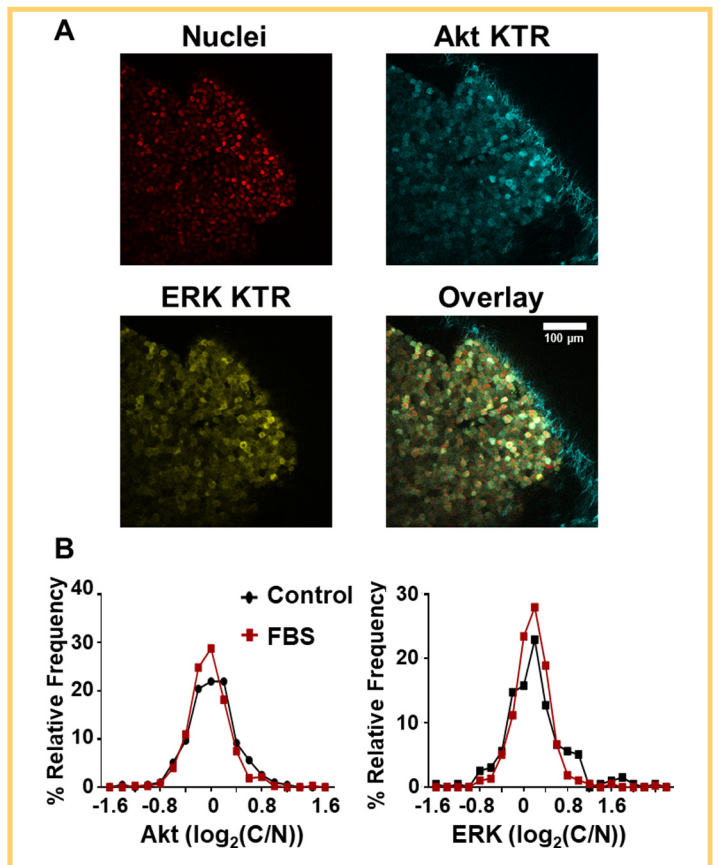


Figure 8. Conditioning does not alter activities of Akt or ERK in breast cancer cells immediately after injection into mammary fat pads. Representative images of 10^6 MDA-MB-231 cells conditioned for 4 hours with FBS and then imaged by 2-photon microscopy within 15 minutes of injection into the left fourth mammary fat pad (A). Breast cancer cells stably express fluorescent kinase translocation reporters (KTRs) for Akt (aquamarine) and ERK (mCitrine) with H2B-mCherry marking nuclei. Representative histograms show frequency distributions of the cytoplasmic-to-nuclear ratios (CNR) of the Akt KTR (left) and ERK KTR (right) in MDA-MB-231 cells after conditioning with FBS ($n > 370$ cells) or control ($n > 195$ cells) (B). Three different tumors from each group were analyzed.

difference in the growth of spontaneous metastases. By comparison, intracardiac injection directly introduces breast cancer cells into the systemic circulation immediately after conditioning, so cellular memory can affect the initial proliferation of cells in an organ or tissue. Further investigation will be required to identify potential causes of site-specific effects of conditioning on tumor progression and metastasis.

To identify possible mechanisms for enhanced tumor initiation, we assessed effects of conditioning on cellular proliferation,

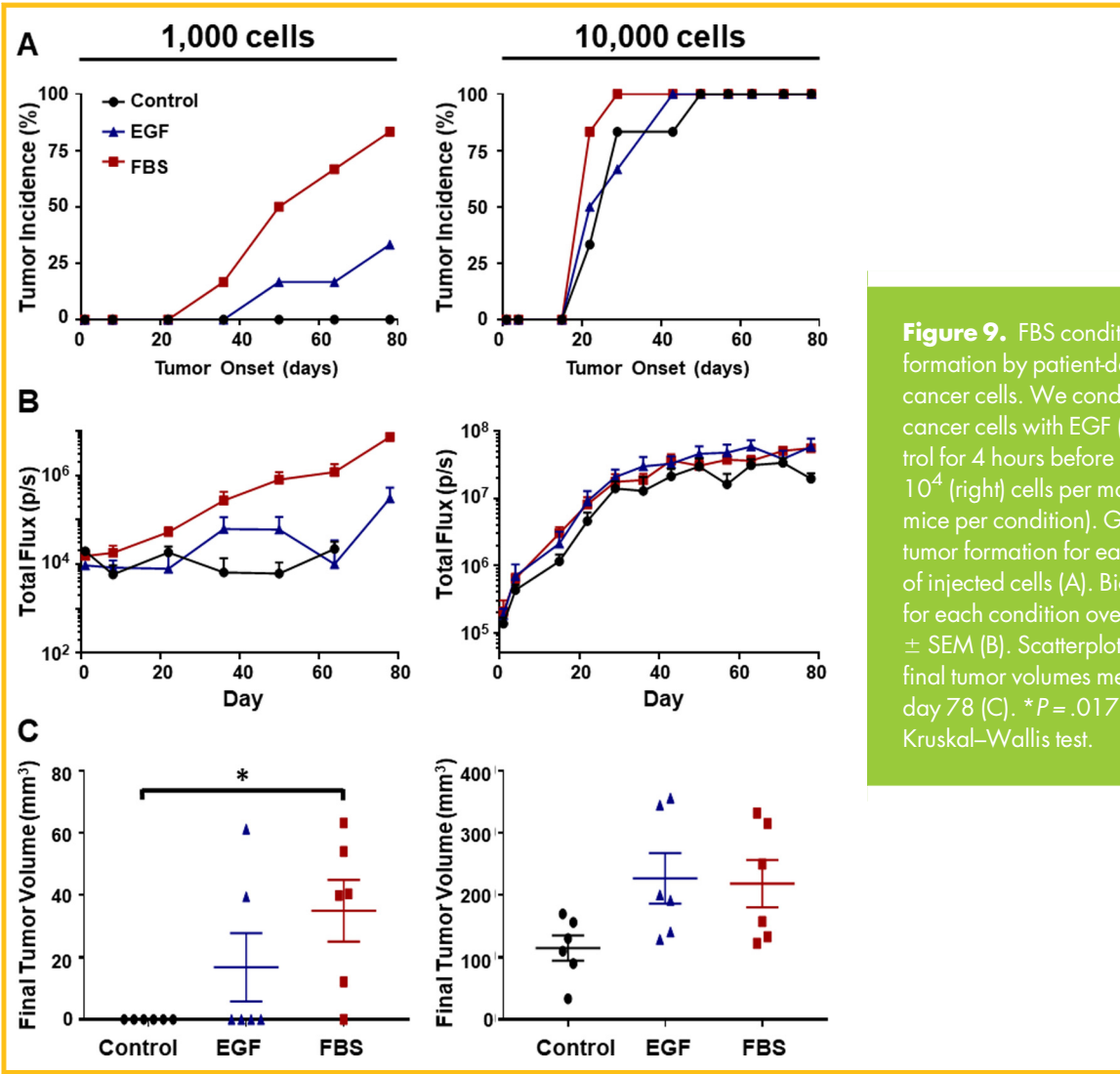


Figure 9. FBS conditioning promotes tumor formation by patient-derived Vari-068 breast cancer cells. We conditioned Vari-068 breast cancer cells with EGF (300 ng/mL), FBS, or control for 4 hours before implanting 10^3 (left) or 10^4 (right) cells per mammary fat pad (n = 3 mice per condition). Graphs show incidences of tumor formation for each condition and amount of injected cells (A). Bioluminescence imaging for each condition over time expressed as mean \pm SEM (B). Scatterplots with mean \pm SEM for final tumor volumes measured by calipers on day 78 (C). * $P = .017$ for FBS versus control by Kruskal–Wallis test.

adhesion, and signaling in the mammary fat pads immediately after injection. None of these candidate regulators of tumor initiation showed significant differences among groups. Potentially, our cell-based assays of proliferation and adhesion failed to capture key components of the tumor microenvironment in vivo. Because tumor initiation requires as few as 1 cell, population-

scale assays may not identify critical subpopulations of cells that drive formation of a tumor. Future studies with approaches that better define changes in single cells, such as shifts in frequencies of cancer stem cells, may reveal cellular and molecular mechanisms for effects of conditioning stimuli on incidence of tumor formation.

We acknowledge other limitations of this work. We utilized injections of cancer cells into bilateral mammary fat pads, so cells in 1 site potentially influenced breast cancer cells injected into the other fat pad. However, we did not notice a consistent pattern in tumor growth between 2 tumors in an individual mouse. Although bioluminescence imaging offers improved sensitivity compared with other whole-animal techniques such as magnetic resonance imaging or computed tomography, detection of small numbers of cells (~100 or fewer) remains challenging, particularly in metastatic sites. Intravital microscopy for kinase signaling achieves single-cell resolution, but depth limitations of this method constrain the total numbers of cells analyzed. We did not implant human stromal cells along with the breast cancer cells, which would better mimic the tumor microenvironment in humans. In addition,

Table 5. Tumor Formation of Vari-068 Cells at Different Cell Dosages after Conditioning at Different Cell Dosages^a

Condition	Number of Cells Injected	
	10^3	10^4
Control	0/6 (0%)	6/6 (100%)
FBS	5/6 (83%)*	6/6 (100%)
EGF	2/6 (33%)	6/6 (100%)

* $P = .0152$ versus control by Fisher exact test.

^a Displayed as number of tumors formed/number of injections (percent tumors formed).

we used immunocompromised mice to study human breast cancer cells, so we did not investigate potential regulation of tumor formation by the immune system.

In summary, we demonstrated that short-term changes in growth factors and nutrients that occur in tumors can drive longer-term tumorigenic behavior based on cellular memory. The potential for targeted inhibitors such as

ridaforolimus to increase tumor-initiating potential of breast cancer cells requires further investigation to determine the effects on treatment failures and delayed recurrences in patients. Understanding how transient signals impart cellular memory to cancer cells that regulate tumor formation and progression ultimately may lead to new drug targets and more effective use of existing therapies.

ACKNOWLEDGMENTS

The authors acknowledge funding from United States National Institutes of Health grants R01CA238042, R01CA196018, U01CA210152, R01CA238023, R33CA225549, R50CA221807, and R37CA222563. B.A.H. receives support from an American Cancer Society—Michigan Cancer Research Fund Postdoctoral Fellowship, PF-18-236-01-CCG. J.M.B. is supported by National Science Foundation Graduate Research Fellowship Grant No. DGE 1256260.

Author Contributions: S.S.E., K.E.L., and G.D.L. conceptualized and designed the study. B.A.H. and K.E.L. provided reagents. S.S.E., J.M.B., B.A.H., and T.H.R. performed the experiments. S.S.E. and K.E.L. analyzed the data. S.S.E. and G.D.L. wrote the manuscript. All authors reviewed the manuscript prior to submission.

Competing Interests: G.D.L. serves as a consultant and receives research funding from Polyphor. All other authors declare no competing interests.

REFERENCES

1. Gillies RJ, Schomack PA, Secomb TW, Raghunand N. Causes and effects of heterogeneous perfusion in tumors. *Neoplasia*. 1999;1:197–207. doi:10.1038/sj.neo.7900037
2. Brurberg KG, Benjaminsen IC, Dorum LM, Rofstad EK. Fluctuations in tumor blood perfusion assessed by dynamic contrast-enhanced MRI. *Magn Reson Med*. 2007;58:473–481. doi:10.1002/mrm.21367
3. Baudelet C, Ansiaux R, Jordan BF, Havaux X, Macq B, Gallez B. Physiological noise in murine solid tumours using T2*-weighted gradient-echo imaging: A marker of tumour acute hypoxia? *Phys Med Biol*. 2004;49:3389–3411.
4. Trotter MJ, Chaplin DJ, Durand RE, Olive PL. The use of fluorescent probes to identify regions of transient perfusion in murine tumors. *Int J Radiat Oncol Biol Phys*. 1989;16:931–934.
5. Hanahan D, Weinberg RA. Hallmarks of cancer: the next generation. *Cell*. 2011;144:646–674. doi:10.1016/j.cell.2011.02.013
6. Carmeliet P, Jain RK. Principles and mechanisms of vessel normalization for cancer and other angiogenic diseases. *Nat Rev Drug Discov*. 2011;10:417–427. doi:10.1038/nrd3455
7. Helmlinger G, Yuan F, Dellian M, Jain RK. Interstitial pH and pO₂ gradients in solid tumors in vivo: high-resolution measurements reveal a lack of correlation. *Nat Med*. 1997;3:177–182.
8. Sutherland RM. Cell and environment interactions in tumor microregions: the multicell spheroid model. *Science*. 1988;240:177–184. doi:10.1126/science.2451290
9. Muz B, de la Puente P, Azab F, Azab AK. The role of hypoxia in cancer progression, angiogenesis, metastasis, and resistance to therapy. *Hypoxia (Auckl)*. 2015;3:83–92. doi:10.2147/HP.S93413
10. Casciari JJ, Sotirchos SV, Sutherland RM. Variations in tumor cell growth rates and metabolism with oxygen concentration, glucose concentration, and extracellular pH. *J Cell Physiol*. 1992;151:386–394. doi:10.1002/jcp.1041510220
11. Lewis DM, Park KM, Tang V, Xu Y, Pak K, Eisinger-Mathason TSK, Simon MC, Gerecht S. Intratumoral oxygen gradients mediate sarcoma cell invasion. *Proc Natl Acad Sci USA*. 2016;113:9292–9297. doi:10.1073/pnas.1605317113
12. Carmona-Fontaine C, Deforet M, Akkari L, Thompson CB, Joyce JA, Xavier JB. Metabolic origins of spatial organization in the tumor microenvironment. *Proc Natl Acad Sci USA*. 2017;114:2934–2939. doi:10.1073/pnas.1700600114
13. Ishida T. Investigation of the Influence of Glucose Concentration on Cancer Cells by Using a Microfluidic Gradient Generator without the Induction of Large Shear Stress. *Micromachines (Basel)*. 2016;7. pii: E155. doi:10.3390/mi7090155
14. Kimura H, Braun RD, Ong ET, Hsu R, Secomb TW, Papahadjopoulos D, Hong K, Dewhirst MW. Fluctuations in red cell flux in tumor microvessels can lead to transient hypoxia and reoxygenation in tumor parenchyma. *Cancer Res*. 1996;56:5522–5528.
15. Brown JM. The hypoxic cell: a target for selective cancer therapy—eighteenth Bruce F. Cain Memorial Award lecture. *Cancer Res*. 1999;59:5863–5870.
16. Parliament MB, Chapman JD, Urtasun RC, McEwan AJ, Golberg L, Mercer JR, Mannan RH, Wiebe LJ. Non-invasive assessment of human tumour hypoxia with 123I-iodoazomycin arabinoside: preliminary report of a clinical study. *Br J Cancer*. 1992;65:90–95. doi:10.1038/bjc.1992.17
17. Jain RK. Delivery of molecular and cellular medicine to solid tumors. *Adv Drug Deliv Rev*. 2012;64:353–365. doi:10.1016/j.addr.2012.09.011

18. Minassian LM, Cotechini T, Huitema E, Graham CH. Hypoxia-induced resistance to chemotherapy in cancer. *Adv Exp Med Biol*. 2019;1136:123–139. doi:10.1007/978-3-030-12734-3_9
19. Herrmann A, Rice M, Lévy R, Pizer BL, Losty PD, Moss D, Sée V. Cellular memory of hypoxia elicits neuroblastoma metastasis and enables invasion by non-aggressive neighbouring cells. *Oncogenesis*. 2015;4:e138. doi:10.1038/oncis.2014.52
20. Mathis R, Ackermann M. Asymmetric cellular memory in bacteria exposed to antibiotics. *BMC Evol Biol*. 2017;17:73. doi:10.1186/s12862-017-0884-4
21. Celià-Terrasa T, Bastian C, Liu DD, Ell B, Aiello NM, Wei Y, Zamalloa J, Blanco AM, Hang X, Kunisky D, Li W, Williams ED, Rabitz H, Kang Y. Hysteresis control of epithelial-mesenchymal transition dynamics conveys a distinct program with enhanced metastatic ability. *Nat Commun*. 2018;9:5005. doi:10.1038/s41467-018-07538-7
22. Hillebrand LE, Wickberg SM, Gomez-Auli A, Follo M, Maurer J, Busch H, Boerries M, Reinheckel T. MMP14 empowers tumor-initiating breast cancer cells under hypoxic nutrient-depleted conditions. *FASEB J*. 2019;33:4124–4140. doi:10.1096/fj.2018011127R
23. Mitra T, Menon SN, Sinha S. Emergent memory in cell signaling: persistent adaptive dynamics in cascades can arise from the diversity of relaxation time-scales. *Sci Rep*. 2018;8:13230. doi:10.1038/s41598-018-31626-9
24. Spinosa PC, Humphries BA, Lewin Mejia D, Buschhaus JM, Linderman JJ, Luker GD, Luker KE. Short-term cellular memory tunes the signaling responses of the chemokine receptor CXCR4. *Sci Signal*. 2019;12:eaaw4204. doi:10.1126/scisignal.aaw4204
25. Lopez-Knowles E, O'Toole SA, McNeil CM, Millar EK, Qiu MR, Crea P, Daly RJ, Musgrove AP, Sutherland RL. PI3K pathway activation in breast cancer is associated with the basal-like phenotype and cancer-specific mortality. *Int J Cancer*. 2010;126:1121–1131. doi:10.1002/ijc.24831
26. Cerami E, Gao J, Dogrusoz U, Gross BE, Sumer SO, Aksoy BA, Jacobsen A, Byrne CJ, Heuer ML, Larsson E, Antipin Y, Reva B, Goldberg AP, Sander C, Schultz N. The cBio cancer genomics portal: an open platform for exploring multidimensional cancer genomics data. *Cancer Discov*. 2012;2:401–404. doi:10.1158/2159-8290.CD-12-0095
27. Grob TJ, Heilenkötter U, Geist S, Paluchowski P, Wilke C, Jaenicke F, Quaas A, Wilczak W, Choschzick M, Sauter G, Lebeau A. Rare oncogenic mutations of predictive markers for targeted therapy in triple-negative breast cancer. *Breast Cancer Res Treat*. 2012;134:561–567. doi:10.1007/s10549-012-2092-7
28. Pereira CBL, Leal MF, de Souza CRT, Montenegro RC, Rey JA, Carvalho AA, Assumpção PP, Khayat AS, Pinto GR, Demachki S, de Arruda Cardoso Smith M, Burbano RR. Prognostic and predictive significance of MYC and KRAS alterations in breast cancer from women treated with neoadjuvant chemotherapy. *PLoS One*. 2013;8:e60576. doi:10.1371/journal.pone.0060576
29. Balko JM, Cook RS, Vaught DB, Kuba MG, Miller TW, Bhola NE, Sanders ME, Granja-Ingram NM, Smith JJ, Meszoely IM, Salter J, Dowsett M, Stemke-Hale K, González-Angulo AM, Mills GB, Pinto JA, Gómez HL, Arteaga CL. Profiling of residual breast cancers after neoadjuvant chemotherapy identifies DUSP4 deficiency as a mechanism of drug resistance. *Nat Med*. 2012;18:1052–1059. doi:10.1038/nm.2795
30. Müller A, Homey B, Soto H, Ge N, Catron D, Buchanan ME, McClanahan T, Murphy E, Yuan W, Wagner SN, Barrera JL, Mohar A, Verástegui E, Zlotnik A. Involvement of chemokine receptors in breast cancer metastasis. *Nature*. 2001;410:50–56. doi:10.1038/35065016

31. Smith MCP, Luker KE, Garbow JR, Prior JL, Jackson E, Piwnica-Worms D, Luker GD. CXCR4 regulates growth of both primary and metastatic breast cancer. *Cancer Res.* 2004;64:8604–8612. doi:10.1158/0008-5472.CAN-04-1844
32. Carracedo A, Ma L, Teruya-Feldstein J, Rojo F, Salmena L, Alimonti A, Egia A, Sasaki AT, Thomas G, Kozma SC, Papa A, Nardella C, Cantley LC, Baselga J, Pandolfi PP. Inhibition of mTORC1 leads to MAPK pathway activation through a PI3K-dependent feedback loop in human cancer. *J Clin Invest.* 2008;118:3065–3074. doi:10.1172/jci34739
33. Breuleux M, Klopfenstein M, Stephan C, Doughty CA, Barys L, Maira S-M, Kwiatkowski D, Lane HA. Increased AKT S473 phosphorylation after mTORC1 inhibition is rictor dependent and does not predict tumor cell response to PI3K/mTOR inhibition. *Mol Cancer Ther.* 2009;8:742–753. doi:10.1158/1535-7163.mct-08-0668
34. Mendoza MC, Er EE, Blenis J. The Ras-ERK and PI3K-mTOR pathways: cross-talk and compensation. *Trends Biochem Sci.* 2011;36:320–328. doi:10.1016/j.tibs.2011.03.006
35. Regot S, Hughey JJ, Bajar BT, Carrasco S, Covert MW. High-sensitivity measurements of multiple kinase activities in live single cells. *Cell.* 2014;157:1724–1734. doi:10.1016/j.cell.2014.04.039
36. Maryu G, Matsuda M, Aoki K. Multiplexed fluorescence imaging of ERK and Akt activities and cell-cycle progression. *Cell Struct Funct.* 2016;41:81–92. doi:10.1247/csf.16007
37. Luo M, Shang L, Brooks MD, Jiagge E, Zhu Y, Buschhaus JM, Conley S, Fath MA, Davis A, Gheordunescu E, Wang Y, Harouaka R, Lozier A, Triner D, McDermott S, Merajver SD, Luker GD, Spitz DR, Wicha MS. Targeting breast cancer stem cell state equilibrium through modulation of redox signaling. *Cell Metab.* 2018;28:69–86.e6. doi:10.1016/j.cmet.2018.06.006
38. Gilani RA, Phadke S, Bao LW, Lachacz EJ, Dziubinski ML, Brandvold KR, Steffey ME, Kwarcinski FE, Graveel CR, Kidwell KM, Merajver SD, Soellner MB. UM-164: a potent c-Src/p38 kinase inhibitor with in vivo activity against triple-negative breast cancer. *Clin Cancer Res.* 2016;22:5087–5096. doi:10.1158/1078-0432.CCR-15-2158
39. Majumder M, Xin X, Liu L, Tutunea-Fatan E, Rodriguez-Torres M, Vincent K, Postovit L-M, Hess D, Lala PK. COX-2 induces breast cancer stem cells via EP4/PI3K/AKT/NOTCH/WNT axis. *Stem Cells.* 2016;34:2290–2305. doi:10.1002/stem.2426
40. Luo M-L, Gong C, Chen C-H, Hu H, Huang P, Zheng M, Yao Y, Wei S, Wulf G, Lieberman J, Zhou XZ, Song E, Lu KP. The Rab2A GTPase promotes breast cancer stem cells and tumorigenesis via Erk signaling activation. *Cell reports.* 2015;11:111–124. doi:10.1016/j.celrep.2015.03.002
41. Grilley-Olson JE, Bedard PL, Fasolo A, Cornfeld M, Cartee L, Razak ARA, Stayner L-A, Wu Y, Greenwood R, Singh R, Lee CB, Bendell J, Burris HA, Del Conte G, Sessa C, Infante JR. A phase Ib dose-escalation study of the MEK inhibitor trametinib in combination with the PI3K/mTOR inhibitor GSK2126458 in patients with advanced solid tumors. *Invest New Drugs.* 2016;34:740–749. doi:10.1007/s10637-016-0377-0
42. Shapiro GI, et al. Phase Ib study of the MEK inhibitor cobimetinib (GDC-0973) in combination with the PI3K inhibitor pictilisib (GDC-0941) in patients with advanced solid tumors. *Invest New Drugs.* 2016;34:740–749. doi:10.1007/s10637-016-0377-0
43. Shimizu T, Tolcher AW, Papadopoulos KP, Beeram M, Rasco DW, Smith LS, Gunn S, Smetzer L, Mays TA, Kaiser B, Wick MJ, Alvarez C, Cavazos A, Mangold GL, Patnaik A. The clinical effect of the dual-targeting strategy involving PI3K/AKT/mTOR and RAS/MEK/ERK pathways in patients with advanced cancer. *Clin Cancer Res.* doi:10.1158/1078-0432.Ccr-11-23812012;18).
44. Humphries BA, Buschhaus JM, Chen Y-C, Haley HR, Qyli T, Chiang B, Shen N, Rajendran S, Cutter A, Cheng Y-H, Chen Y-T, Cong J, Spinosa PC, Yoon E, Luker KE, Luker GD. Plasminogen activator inhibitor 1 (PAI1) promotes actin cytoskeleton reorganization and glycolytic metabolism in triple-negative breast cancer. *Mol Cancer Res.* 2019;17:1142–1154. doi:10.1158/1541-7786.mcr-18-0836
45. Luker KE, Gupta M, Luker GD. Imaging CXCR4 signaling with firefly luciferase complementation. *Anal Chem.* 2008;80:5565–5573. doi:10.1021/ac8005457
46. Luker KE, Mihalko LA, Schmidt BT, Lewin SA, Ray P, Shcherbo D, Chudakov DM, Luker GD. In vivo imaging of ligand receptor binding with Gaussia luciferase complementation. *Nat Med.* 2012;18:172–177. doi:10.1038/nm.2590
47. Stacer AC, Wang H, Fenner J, Dosch JS, Salomonson A, Luker KE, Luker GD, Rehemtulla A, Ross BD. Imaging reporters for proteasome activity identify tumor- and metastasis-initiating cells. *Mol Imaging.* 2015;14:414–428.
48. Ray P, Stacer AC, Fenner J, Cavnar SP, Meguiar K, Brown M, Luker KE, Luker GD. CXCL12-gamma in primary tumors drives breast cancer metastasis. *Oncogene.* 2015;34:2043–2051. doi:10.1038/onc.2014.157